Journal of Fluids and Structures 17 (2003) 1017–1033

JOURNAL OF FLUIDS AND STRUCTURES

www.elsevier.nl/locate/jnlabr/yjfls

Oscillations of a vertical elastically mounted cylinder in a wave: imaging of vortex patterns

K. Downes, D. Rockwell*

Department of Mechanical Engineering and Mechanics, Lehigh University, 354 Packard Laboratory, 19 Memorial Drive West, Bethlehem, PA 18015 3085, USA

Received 6 January 2002; accepted 9 April 2003

Abstract

A vertical, elastically mounted cylinder undergoes two-dimensional oscillations in a free-surface water wave. The cylinder has nonpreferential stiffness and a very low mass-damping parameter. Low damping is accomplished using a mini-jet air bearing system. Patterns of instantaneous vorticity are characterized in a horizontal plane using a technique of high-image-density particle image velocimetry (PIV) involving a two-camera system to preclude the effects of cylinder blockage during image acquisition. A generic trajectory of the cylinder oscillation is generated by tuning the ratio of the natural frequency of the cylinder to the wave frequency; this trajectory is representative of those measured in previous related experiments, for which quantitative flow visualization was not performed. In this investigation, a concept of relative wave velocity provides the most insightful link between the wave motion and the quantitative patterns of vortex generation and interaction; these features are characterized in relation to the instantaneous phase of the cylinder during its trajectory. Basic mechanisms of the vorticity patterns involve: (i) generation of large-scale concentrations of vorticity; (ii) short-duration Kármán shedding; (iii) migration of large-scale concentrations about the periphery of the cylinder; and (iv) collision and distension of previously generated vorticity concentrations with the surface of the cylinder. The states of vortex formation are fundamentally different on each of the branches of the generic cylinder trajectory, even though it has nearly symmetrical left and right branches. Furthermore, it is demonstrated that the vorticity concentrations decay extremely rapidly, which means that the in-plane vortex dynamics are essentially confined to the region close to the cylinder.

1. Introduction

Flow-induced vibration of bluff-bodies has been a subject of considerable experimental study in recent decades. The loading and response of an elastically mounted cylinder, either in a steady current, and in a wave system, or a combination of current and waves, is of obvious importance to the configurations of long cables and offshore structural components. Particularly intriguing is the vibrational response of an elastically mounted cylinder in a wave system, where the direction and magnitude of the wave velocity undergo large excursions in magnitude and direction, thereby leading to potentially complex loading and elastic response of the cylinder system.

In the following, relevant parameters are defined, and then the case of a stationary cylinder in oscillatory flow is addressed, followed by a review of elastic cylinder systems in simulated and actual waves, interpreted in conjunction with cylinder trajectories and vortex patterns during bidirectional motion. These considerations lead to definition of the unresolved issues and objectives for this class of flow-structure interaction.

*Corresponding author. Tel.: +1-610-758-4107; fax: +1-610-758-4041.
E-mail address: dor0@lehigh.edu (D. Rockwell).

0889-9746/03/$ - see front matter
doi:10.1016/S0889-9746(03)00055-0

1.1. Parameter definitions and concepts

Two dimensionless parameters of central importance in classifying self-excited vibrations of a cylinder in a wave are the Keulegan–Carpenter number, KC, and the so-called beta parameter, β. The Keulegan–Carpenter number is defined as

$$\mathrm{KC} = \frac{U_m}{fD}, \tag{1}$$

where U_m is the velocity amplitude of the flow past the cylinder, f is the wave frequency, and D is the diameter of the cylinder. The Stokes number is defined as

$$\beta = \frac{fD^2}{v}, \tag{2}$$

where v is the kinematic viscosity. The Reynolds number Re is defined as $\mathrm{Re} = \mathrm{KC} \cdot \beta$.

When the cylinder vibrates, it is necessary to define the mass-damping parameter, $m^*\varsigma$, in which

$$m^* = \frac{m_{\mathrm{sys}}}{m_d}, \tag{3}$$

$$\varsigma = \frac{C_{\mathrm{sys}}}{C_{\mathrm{crit}}} = \frac{C_{\mathrm{sys}}}{2\sqrt{m_{\mathrm{sys}}k}}, \tag{4}$$

where m_{sys} is the system mass, m_d is the mass displaced by the fluid, C_{sys} is the system damping in air, C_{crit} is the critical damping, and k is the spring stiffness. The mass-damping parameter describes vibrating systems and is inversely proportional to the amplitude of vibration. It is desirable to achieve the lowest mass-damping possible to ensure relevance to real engineering applications. It should be noted that the mass-damping parameter multiplied by $4/\pi$ is equivalent to a stability parameter defined by Isaacson and Maull (1981).

Another important parameter for the elastic system is the frequency ratio, f_n/f_w, in which f_n is the natural frequency in water and f_w is the wave frequency. Section 1.4 discusses the significance of the frequency ratio in further detail.

1.2. Stationary cylinder in oscillatory flow

A wide variety of previous investigations have studied the loading of stationary cylinders in unidirectional oscillatory flow. Sarpkaya and Isaacson (1981) summarized early studies over a range of KC number. Investigations include Honji (1981), Bearman et al. (1981), Ikeda and Yamamoto (1981), Iwagaki et al. (1983), Williamson (1985a), Sarpkaya (1986), and Obasaju et al. (1988). Tatsuno and Bearman (1990) is an example of an investigation that approximated the above condition by mechanically oscillating a cylinder in quiescent fluid. These investigations provided insight into the vortex patterns that can arise over various ranges of KC and, in certain cases, their relationship to the cylinder loading.

1.3. Elastic cylinder systems in simulated and actual waves

Vibration of elastically mounted cylinders in simulated and actual waves has been addressed in a variety of investigations. Simulated wave motion has involved either unidirectional oscillatory flow past the cylinder, typically generated using a U-tube arrangement, or forced oscillation of the elastic cylinder system in quiescent fluid. Actual wave motion involves regular progressive waves, typically of the intermediate and deep categories. In the following, investigations involving three categories of elastically mounted cylinders are considered: elastic vibration only in the transverse (crosswave) direction; in the in-line direction; and bidirectional vibration, which allows simultaneous motion in the transverse and in-line directions. An overview of all three cases can be found in Sumer and Fredsøe (1997).

1.3.1. Transverse vibration

Early investigations employed a U-tube arrangement to generate unidirectional (nonorbital) oscillatory flow past an elastically supported cylinder, which was free to vibrate in the transverse direction. Sarpkaya and Rajavi (1979) demonstrated the occurrence of lock-on of the cylinder response at a given value of reduced velocity. Bearman and Hall (1987) characterized the response over a range of KC number $\mathrm{KC} = U_n/f_w D$ and frequency ratio f_n/f_w, in which f_w is the simulated wave frequency, i.e. the oscillation frequency of water in the U-tube. They defined the natural frequency of the cylinder based on vibrations in water, as opposed to the frequently used definition based on vibrations in air, and

found that resonant response of the cylinder motion occurred at integer values of f_n/f_w. Employing forced oscillations in quiescent fluid, Sumer and Fredsøe (1988) and Kozakiewicz et al. (1997) addressed the frequency and amplitude response of the cylinder vibration in terms of the ratio of cylinder vibration frequency f_v, to the equivalent wave frequency f_w.

For the case of a cylinder subjected to an actual free-surface wave, its transverse response exhibits certain similarities to the foregoing observations. Angrilli and Cossalter (1982) found that resonant response occurs at integer values of frequency ratio f_n/f_w. In a similar type of wave tank, Kaye and Maull (1993) found that the peak transverse response occurs at $f_n/f_w = 2$ and, remarkably enough, does not appear to be significantly influenced when motion of the cylinder is allowed in the in-line direction. Most recently, Hayashi and Chaplin (1998) further characterized the occurrence of resonant response at integer values of f_n/f_w. They also found, however, that coupled response with the vortex formation can occur even when the oscillation frequency is not an integer of f_w, provided the spring-cylinder system has light damping.

1.3.2. *In-line vibration*

Williamson (1985b) successfully predicted resonant in-line vibrations of a cylinder by formulating an equation of motion involving the Morison equation for flow-induced, in-line forces. The model was verified by unidirectional oscillatory experiments. Li et al. (1997) performed a theoretical analysis and experiments for a horizontal, elastically mounted cylinder. Both regular and random wave motion were simulated, and their results were interpreted in terms of the ratio of the natural frequency f_n to the wave frequency f_w. Anagnostopoulos et al. (1995) undertook a numerical simulation of in-line oscillations in a simulated unidirectional wave motion, analogous to that occurring experimentally in a U-tube. Their investigation focused on lower values of KC. Provided the dimensionless wave amplitude is sufficiently small, they indicate that the in-line response can be well predicted.

1.3.3. *Bidirectional vibrations*

The possibility of simultaneous transverse and in-line vibrations of the cylinder, i.e. bidirectional vibrations, has been addressed using two basic types of configurations. The first involves a rigid cylinder attached to a bidirectional cantilevered joint or flexible joint at the bottom surface of a wave tank, and the second employs a rigid, horizontal cylinder spring-supported at either end.

Representative investigations of the first category include Sawaragi et al. (1977), Isaacson and Maull (1981), Zedan et al. (1981), Borthwick and Herbert (1988), and Kaye and Maull (1993). Sawaragi et al. classified the maximum response in the transverse and in-line directions as a function of frequency ratio f_n/f_w. The largest amplitude of the in-line response was at $f_n/f_w = 1$ when $KC < 3$, while the largest response in the transverse direction was at $f_n/f_w = 2$ and 3 when $KC > 3$. Remarkably, the maximum in-line amplitude was of the same order as the maximum transverse amplitude. A number of types of Lissajous trajectories, $y(t)$ versus $x(t)$ were observed as a function of f_n/f_w and KC. Isaacson and Maull (1981) considered variations of: frequency ratio f_n/f_w; wave depth parameter kd; mass ratio $m/\rho D^2$; and KC number. They find that the transverse oscillation amplitude was inversely related to a stability parameter, which is proportional to the mass-damping parameter. The system also exhibited large transverse oscillations at twice the wave frequency as the frequency ratio approached $f_n/f_w = 2$ and when KC is between 10 and 15. Zedan et al. (1981) employed a bidirectional joint of the cantilevered type, and found the response energy to be centered at the wave frequency and, to a lesser extent, at the shedding frequency, which was twice the wave frequency f_w. As lock-in was approached, the response occurred at a single frequency centered at the shedding frequency, and the in-line of the response was amplified substantially. Kaye and Maull (1993) found the maximum transverse response at $f_n/f_w = 2$ and maximum in-line response tended to occur at $f_n/f_w = 1$, although their system could not achieve this frequency ratio. For a similar bidirectional, cantilevered system, Borthwick and Herbert (1988) characterized the resonant response in terms of integer ratios of f_n/f_w and, furthermore, found that the force coefficients in the in-line and transverse directions were dependent upon the orbital shape parameter Ω of the cylinder trajectory when $KC \geqslant 14$, represented by Lissajous plots of $y(t)$ versus $x(t)$. The predominant in-line response and force occurred at the wave frequency f_w.

An alternate configuration, relative to the foregoing, is a rigid horizontal cylinder spring supported at its ends, as employed by Lipsett and Williamson (1991, 1994). They simulated the wave motion by unidirectional oscillatory flow in a U-tube system, and the cylinder was mounted at either end on a four-spring arrangement, in order to allow bidirectional response. A variety of cylinder trajectories $y(t)$ versus $x(t)$ were observed and classified on the basis of maps of KC versus f_n/f_w. Correspondingly, simple mathematical models were invoked in efforts to predict the limit cycle trajectories of the cylinder response.

Irrespective of the type of configuration of the elastic cylinder, common dimensionless parameters are appropriate. In addition to the important parameters of frequency ratio f_n/f_w and KC number described in the foregoing investigations,

the effects of mass-damping parameter $m^*\varsigma$ should be specified. Typical values of the mass-damping parameter for the aforementioned bidirectional systems are: $m^*\varsigma =$ in the range of 0.044–0.44 (Isaacson and Maull, 1981), 0.095 (Borthwick and Herbert, 1988), and 0.037 (Kaye and Maull, 1993). Although the value of the mass-damping parameter could not be deduced from the work of Zedan et al. (1981), it is likely large due to use of solid aluminum construction and a top flange device. Sawaragi et al. (1977) did not indicate cylinder mass, but damping was specified at $\varsigma = 0.00796$. Lipsett and Williamson (1991, 1994) estimated mass damping due to damping in water to be $m^*\varsigma = 0.05$; damping in air was not addressed, due to their arrangement.

1.4. Cylinder trajectories and vortex patterns during bidirectional motion

Taken together, the Lissajous trajectories $y(t)$ versus $x(t)$ of Sawaragi et al. (1977), Borthwick and Herbert (1988), and Lipsett and Williamson (1991, 1994) reveal an interesting array of possible motions of the cylinder when $KC < 20$. For example, Sawaragi et al. (1977) employed values of KC up to 15, showing that when the frequency ratio f_n/f_w approaches unity, a diagonal (oval) pattern occurred with amplified displacement in the in-line direction. As f_n/f_w approached 2, a "butterfly" pattern emerged with two oscillations in the transverse direction for every oscillation in the in-line direction. In this case, the transverse vibration was more pronounced than the in-line vibration. A similar pattern occurred for $f_n/f_w = 3$, except that there were three oscillations in the transverse direction for every oscillation in the in-line direction. Borthwick and Herbert (1988) presented similar types of trajectories, and interpreted them with measurements of the transverse and in-line force variations as a function of time. For a frequency ratio of 2, the authors found the strongest resonance at $KC = 11.5$. In the investigation of Lipsett and Williamson (1991, 1994), certain features of their trajectories are in common with the aforementioned. They considered values of KC ranging from 2.5 to 20 with f_n/f_w extending from 1.1 to 8.6 and characterized both repeatable and inconsistent trajectories. As a result, a great variety of trajectories were obtained. It appears, however, that when the ratio f_n/f_w takes on integer values, the trajectories exhibit fundamentally common characteristics, that is, repeatable amplified and coupled transverse and in-line vibration with the number of transverse oscillations corresponding to the number of vortices shed per cycle.

Vortex patterns related to these bidirectional trajectories of the cylinder have been deduced from qualitative visualization of the free surface. Borthwick and Herbert (1988) found, from their free-surface observations, that residual vortices shed from previous cycles interacted with the cylinder during its resonant, large-amplitude vibrational response. Kaye (1989) compared free-surface vortices from the stationary cylinder with those formed from a vibrating cylinder. For the latter, previously shed vortices collided with the cylinder, while for the former, they did not.

1.5. Unresolved issues and objectives

It is generally acknowledged that consistent, organized oscillations of an elastically mounted cylinder are optimized when the axis of the cylinder remains orthogonal to the direction of the incident unsteady or steady flow. Yet, for previous investigations that have focused on bidirectional oscillations in a simulated or an actual wave, the cylinder motion has been in a mode that involves tilting, bending or flexing in some manner relative to a fixed pivot point. Moreover, it is generally accepted that the peak amplitude of oscillation, as well as the breadth of the lock-on response of the oscillating cylinder are maximized when the mass-damping ratio is minimal. To date, all bidirectional elastic systems have involved mass-damping ratios that have moderate or relatively high magnitudes. The challenge, therefore, is to implement a bidirectional elastic system having very low mass-damping ratio that simultaneously preserves orthogonality between the cylinder axis and the incident wave direction during an entire oscillation cycle.

The nature of vortex formation and interaction during the trajectory of the cylinder motion is a central issue. It is, of course, intimately related to the onset and persistence of self-sustained, limit-cycle oscillations of the bidirectional cylinder system. Although qualitative visualization of surface vortex patterns has suggested interesting aspects of vortex formation and development, the quantitative nature of these vortices has remained uncharacterized in an experimental sense. Important are the phase shift between the process of vortex formation and the cylinder motion, the nature of vortex–vortex interaction in the region about the cylinder, the possibility of vortex collision or attachment to the cylinder surface, all interpreted with the vorticity distribution and circulation of each concentration of vorticity. In addressing these issues, it would be insightful to interpret the quantitative nature of the vortex system using a relative velocity concept, based on the instantaneous vector velocity of the cylinder during its trajectory, with respect to the instantaneous vector of the wave velocity. This investigation aims to address these features for a generic type of cylinder trajectory in a wave field.

2. Experimental system and techniques

The present experiment addresses self-excited vibration of a vertical cylinder, which is elastically supported and located in a unidirectional free-surface wave. The cylinder is free to move in any direction in the horizontal plane. Particle image velocimetry (PIV) is used to visualize the vortex structures at a defined depth in the wave. Details of the experimental system and techniques are described in the following.

2.1. Wave tank

A custom-designed wave tank constructed entirely of high quality glass allows optical access from an arbitrary direction. Waves are generated by a paddle-type wavemaker at one end; a wedge-shaped beach on the opposite end absorbs the generated wave. The tank is 927 cm long and 42.7 cm wide. The still water level is maintained at 70 cm. The wavemaker, by Edinburgh Design Limited, is constructed in the form of a wedge-shaped aluminum paddle. It is hinged at the bottom edge, and the backside is maintained dry. The hydrostatic force on the wet side is offset by adjustable springs on the dry side. The flap is driven by an electric servomotor. A piezoelectric force transducer measures the load on the paddle, and, via a feedback system, allows reflected energy to be reduced via impedance matching.

The beach has the form of a 125 cm long, 20° wedge, and was constructed of waffle-patterned, acrylic plastic sheets covered by dense floor matting. The interior of the wedge features four additional parallel plastic frames sheathed in the matting and spanning the width of the wedge. Approximately 7 cm × 7 cm, squares of matting fill the remainder of the beach to provide a dense but porous structure. For all beach arrangements employed in wave tanks, including the present one, there is a degree of wave reflection. Even relatively small amplitude reflections based on wave height can induce significant distortion of the particle orbit trajectory, though this effect is not typically characterized. For the wave of primary interest in this investigation, $f_w = 0.5$ Hz and $\lambda = 4.6$ m. The depth to wavelength ratio was $d/\lambda = 0.15$, corresponding to an intermediate wave, between a deep and shallow water wave. Wave reflection from the beach was determined to be at 2% of the incident wave energy, corresponding to 14% of the wave height. For this reason, substantial effort was devoted to characterizing the particle trajectory of the wave, comparing with theory, then locating the cylinder at a node of the wave system, in order to ensure that the major axes of all particle trajectories were horizontal. At the node, the surface wave height was $H = 35$ mm. The actual trajectories were characterized by evaluating instantaneous PIV images of the velocity field at successive phases of the wave motion, then constructing the orbital trajectory. At an elevation centered 2.5 cm beneath the still water level, the elliptical trajectory had major and minor axes of 70 and 34 mm, respectively, corresponding to an orbital ratio of $\Omega = 2.1$. Another orbital trajectory, taken at an elevation centered at 12.5 cm beneath the still water level corresponded to a major and minor axes of 65 and 28 mm, respectively, resulting in an orbital ratio of $\Omega = 2.3$. These trajectories are in close agreement with that predicted from theory, based on the approach of Ippen (1966) for an incident-reflecting wave system. The characteristic KC number based on the major axis of the trajectory, is KC = 8.7 and 8.0 for depths of 2.5 and 12.5 cm, respectively. This is in close agreement with a measured value of KC = 9.1 obtained at a depth of 7.5 cm using an alternative PIV approach and accounting for a small drift in velocity, which is inherent to wave tank systems.

2.2. Cylinder system

A vertical, elastically mounted cylinder system with very low mass-damping ratio was designed and constructed in the Lehigh University Fluid Mechanics Laboratories, as reported by Downes and Rockwell (1998) and Rockwell et al. (2001). This system is illustrated in Figs. 1a and b; the former is an excerpt from Rockwell et al. (2001). The cylinder is free to move in any direction in the horizontal plane due to nearly circumferentially invariant stiffness provided by a four-spring system. With a diameter of 2.54 cm and a height of 85.2 cm, the cylinder is nominally located in the center of the width of the wave tank.

Low damping is achieved via a custom-designed air bearing. Regulated, compressed air at a gauge pressure of 275–410 kPa is transmitted to the interior of a stationary annular air bearing. A total of 240 holes of diameter 0.40 mm were drilled in a pattern of two concentric circles in the top of the air bearing, thereby producing small-scale, vertically oriented jets. The test cylinder is rigidly attached to, and translates with, a hover plate. The cylinder hover plate "floats" on the air cushion above the air bearing. Contact is avoided, so the only damping is due to fluid effects and hysteresis of the springs. Cylinder position measurement technique does not add any damping since a noncontacting method was devised involving an overhead-mounted video camera. This arrangement provides a dimensionless damping parameter, i.e. damping in air divided by the critical damping, of $\varsigma = 0.0035$. In conjunction with low damping, the cylinder remains vertical through its range of motion.

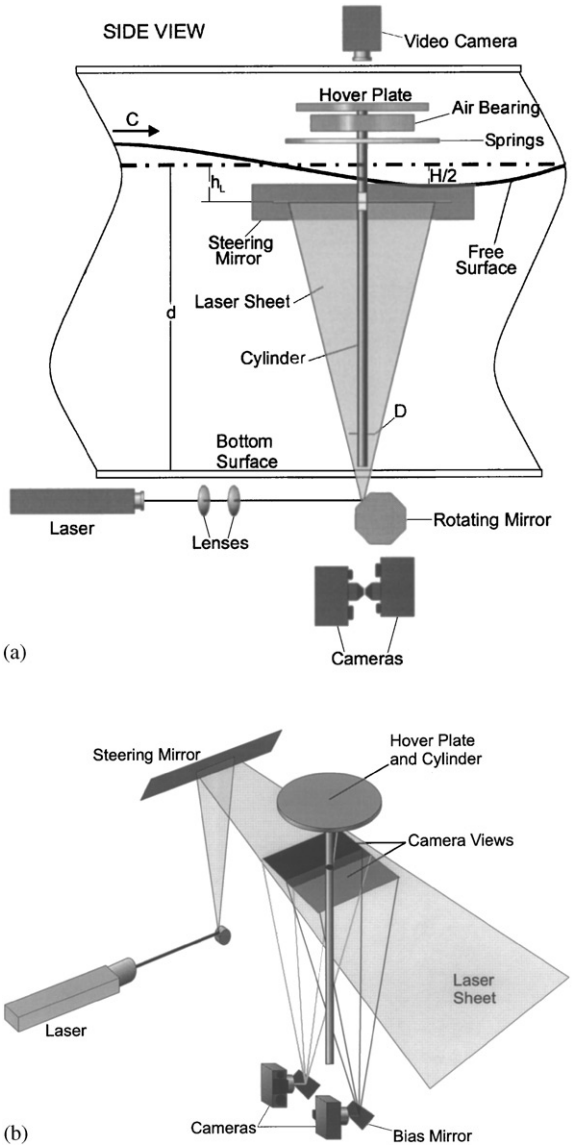

Fig. 1. (a) Schematics illustrating side view of elastically mounted cylinder in conjunction with laser illumination for high-image-density particle image velocimetry. (b) Isometric view of elastic cylinder in wave tank showing orientation of laser sheet relative to fields of view of the two-camera system.

Low mass is obtained by constructing a sealed cylinder from cast acrylic tubing of 2.54 cm outer and 1.95 cm inner diameter. At all junctions, sealant was used to prevent water from entering the interior of the cylinder. The cylinder extends to the floor of the wave tank with a gap of less than 5 mm between the bottom end of the cylinder and the floor. The hover plate consists of two thin-walled aluminum discs on either side of a hexagonal waffle pattern. This design provides a lightweight, rigid system. To allow transmission of the horizontal laser sheet through the cylinder, a water-filled window was employed. The cylindrical wall surrounding the cavity was milled to a thickness of 1.0 mm. The window is centered 7.5 cm below mean water surface level and has a height of 1.4 cm. In addition, a weight at the bottom of the cylinder prevents any measurable tilt of the oscillating cylinder. Both of these features add unavoidable mass to the system, however the dimensionless mass is maintained at $m^* = 1.78$. Therefore the overall mass-damping parameter is $m^*\varsigma = 0.0062$.

A four-spring system provides, to a good approximation, circumferentially invariant stiffness. A detailed discussion of the variance in directional stiffness is provided by Downes (1999). Long (6.35 cm) springs with low stiffness were chosen to increase directional invariance and decrease the natural frequency of the apparatus. The springs are attached to the cylinder via an acrylic bushing at 90° intervals, as well as to a stationary outer annulus. The bushing allows slip between the cylinder and the spring system, thereby preventing the springs from producing a torsional load. Each spring was tested for consistency of stiffness by extension tests under the influence of a fixed mass load.

The natural frequency could be manipulated either by adding more weight to the bottom of the cylinder or by changing the stiffness of the springs. Additional weight has the side effect of changing the dimensionless mass, while different springs affect the dimensionless damping.

2.3. Laser scanning and image acquisition

Two-dimensional, instantaneous velocity fields with high spatial resolution were obtained using the technique of PIV. These two-dimensional fields were then evaluated to generate vorticity distributions.

The PIV technique was based on images of small seeding particles, which were rapidly illuminated by a scanning laser beam from a continuous wave Argon-ion laser manufactured by Coherent Innova. This laser has a 20 W maximum, multi-line beam. Seeding particles are of the neutrally buoyant, metallic-coated glass type with an average diameter of 14 μm.

The laser beam was focused through lenses onto a 72-facet rotating mirror manufactured by Lincoln Laser Corporation. The mirror rotated at 2.5 Hz, which allowed optimal spacing of successive illuminations of a given particle on the photographic image. The selected rotation rate of the mirror provided five to six illuminations of each particle during the time that the camera shutters are open. The laser beam deflected by the rotating mirror appeared as a two-dimensional laser sheet, which was oriented vertically but outside the tank. This scanning sheet encountered a large steering mirror, which deflected it 90° to form a horizontal sheet. The horizontal sheet penetrated through the wave tank at an elevation 7.5 cm below the mean surface level of the tank, and in turn, through the window of the cylinder. This horizontal sheet, which had a thickness of 1 mm, contained the field of view for the camera system.

Imaging of the vortex formation from the oscillating cylinder is particularly challenging. An overhead view of the horizontal laser sheet would have been distorted by the free-surface deflection; moreover, the hover plate would have obstructed it. Two Nikon F4 cameras and their associated bias mirrors were therefore located under the wave tank in order to accommodate the motion of the cylinder, and to avoid obstructing the view due to blockage by the bottom of the cylinder, as illustrated in Fig. 1b. Images on either side of the cylinder, acquired by the two cameras, are combined to provide a single overview image. A thick line on the processed images represents the invalid overlap region of the two images. To increase image clarity, the shutter speed of the cameras was as large as 0.033 s, which decreased the framing rate to 2.92 frames per second. High-density 35 mm Kodak TMAX 400 film with a resolution of 300 lines/mm was used to record the images. One bias mirror was used for each camera; the amplitude and frequency of both bias mirror oscillations were synchronized. These bias mirrors were essential to preclude directional ambiguity. Both cameras were controlled by a computer, as are the bias mirrors; the cameras were triggered to fire 0.022 s after the bias mirrors commenced rotation. Output signals from the cameras were recorded as a function of time on an oscilloscope; a video camera produced a continuous record of the oscilloscope traces. A second video camera simultaneously recorded the cylinder position. Both the oscilloscope traces and the cylinder position are displayed simultaneously using an image splitter system.

Emphasis in this investigation is on the oscillating cylinder. Images corresponding to the corresponding cylinder in the same wave facility at reference values of $KC = 10$ and 18 are given by Yang and Rockwell (2002).

2.4. Image processing and interrogation

A Nikon LS-3510AF 35 mm scanner scanned the developed 35 mm black and white film negatives at a resolution of 125 pixels/mm into a transferable image file (TIF). Using the TIF as input, the average particle displacement between successive laser illuminations was calculated within an interrogation area of 90×90 pixels. The mean number of particles per interrogation area was well within the range of approximately 5–10 particles needed to satisfy the high-image-density criterion defined by Adrian (1991). The pattern of images within each interrogation area was evaluated with a single-frame, cross-correlation technique. A 50% overlap between interrogation areas was employed, in accord with the Nyquist criterion. Software developed in-house was used to evaluate and remove invalid displacement vectors caused by shadows, reflections, or laser sheet distortions in the flow field. A bilinear interpolation algorithm was then applied to the flow field without the invalid vectors. This algorithm takes into account: magnification factor; laser

scanning rate; and bias velocity to calculate velocities from the valid vectors. The field was then smoothed by a Gaussian weighted averaging technique. To minimize distortion of the velocity field, a smoothing parameter of 1.3 was chosen prior to calculation of the vorticity field.

3. Cylinder trajectories

Video recording of the cylinder motion showed results similar to the previous investigations of Sawaragi et al. (1977) and Borthwick and Herbert (1988). Near a frequency ratio of $f_n/f_w = 1$, an oval pattern emerges, and near $f_n/f_w = 2$ a trajectory resembling the outline of a "butterfly" wing is established; this pattern has generic features in relation to those described in the Introduction. Substantially away from integral frequency ratios, the trajectory reverts to in-line displacements.

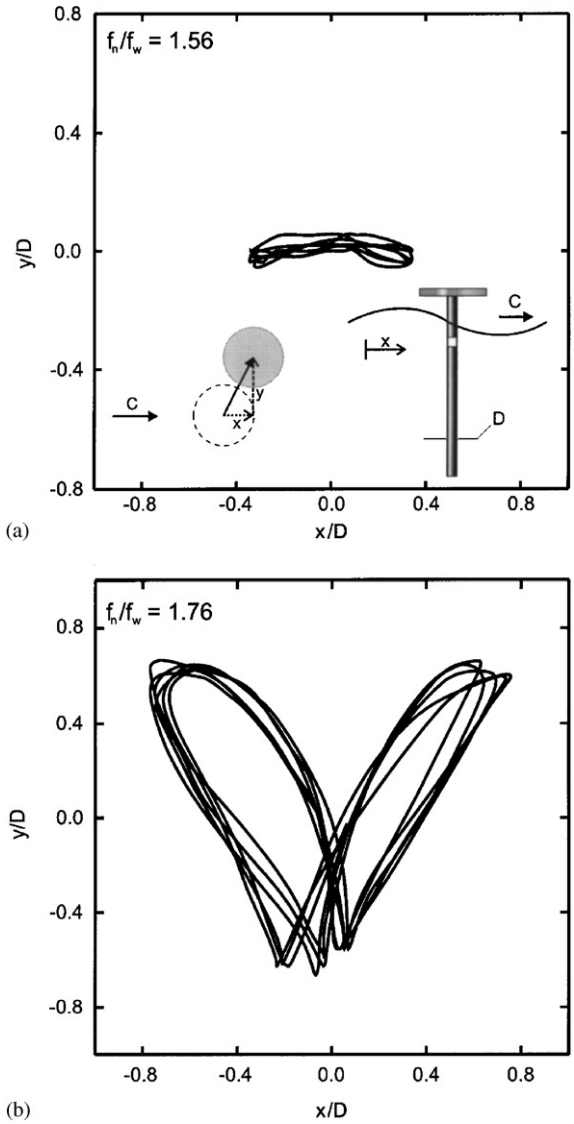

Fig. 2. Trajectories of self-excited motion of cylinder. Upper plot shows motion predominantly in direction of wave motion for KC = 8.2, $\beta = 430$, and ratio of natural frequency in water of elastically mounted cylinder f_n to frequency of wave f_w is $f_n/f_w = 1.56$. Bottom plot exhibits trajectory corresponding to butterfly pattern of cylinder motion for KC = 9.1, $\beta = 380$, and $f_n/f_w = 1.76$.

The upper image in Fig. 2 is a typical example of a nonharmonic response of the cylinder for the case of $f_n/f_w = 1.56$ and $f_{na}/f_w = 1.95$, in which f_n is the natural frequency oscillating in water and f_{na} is the natural frequency oscillating in air. Here KC = 8.2, $\beta = 430$, and six oscillation cycles of the cylinder in the plan view are shown. The in-line and transverse displacements of the cylinder are, respectively, x/D and y/D, normalized by the cylinder diameter. As previously referenced studies infer, the in-line response is small, $x/D < 0.39$ diameters, and the transverse displacements are negligible, $y/D < 0.055$ cylinder diameters.

The lower portion of Fig. 2 shows six oscillation cycles in the plan view of the cylinder for the conditions $f_n/f_w = 1.76$ and $f_{na}/f_w = 2.20$, KC = 9.1, and $\beta = 380$. The repeatable "butterfly" pattern with large transverse and in-line displacements occurs in conjunction with vortex shedding that is harmonically locked to the wave frequency. It should be noted that this steady state, limit-cycle trajectory was established within a few oscillation cycles. Moreover, since the dimensionless mass m^* is low, this pattern could be established over a relatively wide frequency band. At a value of KC ~ 9, the "butterfly" pattern was achieved at frequency ratios of $1.7 < f_n/f_w < 2.0$. The resonant frequency range where the butterfly pattern exists is believed to be larger, but stable wave generation was not possible at higher frequency ratios with the present wave tank–cylinder arrangement. Furthermore, for this trajectory, the amplitudes in the transverse and in-line directions have increased, respectively, to approximately $x/D \sim 0.76$ and $y/D \sim 0.66$ cylinder diameters, relative to those in the upper plot of Fig. 2. Also, the "left" or upstream branch is seen to produce a trajectory encompassing a larger area than the "right" or downstream branch. That is, the left branch is wider than the right branch. As will be addressed in Section 4, the corresponding vortex patterns are different for the left and right branches.

4. Generation and development of vorticity concentrations

The evolution of patterns of vorticity during the generic "butterfly" trajectory of the cylinder is illustrated in Figs. 3a–e, representing frames $N = 1$–9. In each figure, the minimum vorticity level is $\omega_{\min} = 5\,\mathrm{s}^{-1}$, and the incremental level is $\Delta\omega = 2.5\,\mathrm{s}^{-1}$. The inset of each figure shows the overall trajectory of the cylinder for one complete cycle of oscillation. The hollow circles on the trajectory indicate the phases at which sequential images are displayed. The image of interest is designated by the filled (black) symbol. The wave celerity c is in the rightward direction. Positive vorticity, defined to be in the counterclockwise direction, is indicated by bold vorticity contours. All views are in the plan orientation.

4.1. Patterns of vorticity in relation to instantaneous position of cylinder

As shown in Fig. 3a, image $N = 1$ corresponds to an instantaneous velocity V_c of the cylinder (in the laboratory frame) oriented at an angle of $\theta = 60^\circ$. At this instant, the corresponding instantaneous velocity U of the wave is directed to the left and the wave velocity V_R relative to the frame of the cylinder is in a direction $\theta = -64^\circ$. From examination of the cylinder trajectory indicated in the inset, it is evident that the cylinder, at this instant, has just executed an abrupt change in direction.

The three major concentrations of vorticity, labelled A–C in image $N = 1$ (from Rockwell et al., 2001) in Fig. 3a, represent the consequence of the history of the cylinder motion. Negative vortex C was generated during the previous half-cycle, which corresponds to the right branch of the trajectory of the cylinder, shown in the schematic. Moreover, negative vortex A, which was also formed during the motion along the right branch, is in the process of moving away from the surface of the cylinder. Meanwhile, positive vorticity concentrations B develop along the surface of the cylinder. Development of these concentrations A and B occurred when the velocity V_c of the cylinder experienced an abrupt change in angle during the transformation from the right to the left branch of its trajectory. The direction of the wave velocity relative to the cylinder, designated as V_R, is compatible with the separation of concentration A from the surface of the cylinder, inducement of the lower concentration B from the surface, and further development of the upper concentration B.

At a later instant, represented by image $N = 2$, the direction of the velocity V_C of the cylinder is now oriented at $\theta = 155^\circ$ as the cylinder performs the indicated turn on its trajectory. Moreover, the wave velocity V_R relative to the cylinder is oriented to the left at an angle of $\theta = -8^\circ$. The consequence of this change in direction of the cylinder velocity V_C and an increased magnitude of the wave velocity U is to produce a relatively large relative wave velocity V_R that generates the following changes of the patterns of vorticity, relative to those shown in image $N = 1$. First, and most remarkably, new, substantial concentrations of positive D and negative E vorticity have formed on either side of the cylinder surface. Concentration C approaches the surface of the cylinder, and in doing so, it experiences distension as it

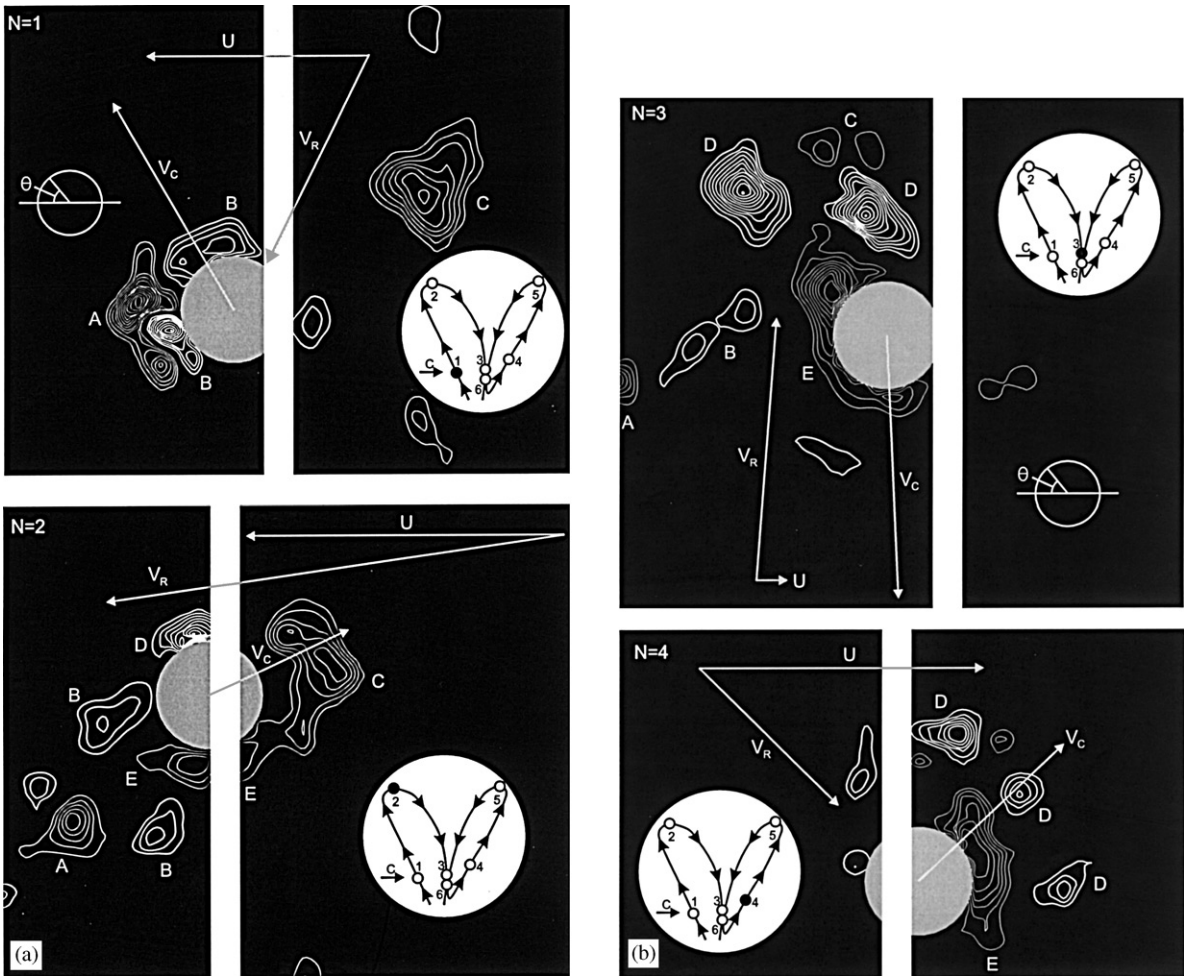

Fig. 3. (a) Patterns of positive (thick line) and negative (thin line) vorticity at instantaneous position of the cylinder represented by (a) images $N = 1$ and 2; (b) images $N = 3$ and 4; (c) images $N = 5$ and 6; (d) images $N = 7$ and 8; (e) images $N = 9$. Minimum vorticity level is $\omega_{\min} = 5\,s^{-1}$ and incremental vorticity is $\Delta\omega = 2.5\,s^{-1}$. Velocity vectors correspond to: V_C = velocity of cylinder; U = particle velocity of undisturbed region of wave adjacent to cylinder; and V_R = relative particle velocity of wave with respect to cylinder.

links with vortex E. Vorticity concentrations A and B have shed from the cylinder and are now well separated from its surface.

At the next location along the cylinder trajectory, represented by image $N = 3$ in Fig. 3b, the cylinder has fully completed its turn in the left branch of its trajectory, and its velocity V_C is now at $\theta = -93^\circ$. Moreover, at this instant, the wave velocity is very small, so the wave velocity V_R relative to the cylinder is oriented at $\theta = 94^\circ$, i.e., nearly perpendicular to the direction of wave motion. Comparison with image $N = 2$ shows that the relative wave velocity V_R has undergone a substantial change in orientation; it has rotated in the clockwise direction by 102°. During this process of reorientation of V_R, concentrations D have fully shed from the cylinder. Remnants of concentration C, which has decayed substantially, exhibit a very low level of vorticity. Vorticity concentration E, which started to form in the previous image, has rotated around to the opposite side of the cylinder from its original position in image $N = 2$, while showing an enhanced level of vorticity. Finally, vorticity concentrations A and B remain well away from the cylinder surface.

Subsequent motion of the cylinder involves an abrupt change in direction, as indicated in the schematic of the inset of image $N = 4$ in Fig. 3b. At this instant, the cylinder velocity V_C is at an angle of 137°. The relative wave velocity V_R has rotated in the clockwise direction to an angle of -136°, which is a rotation of 130° from its position in the previous

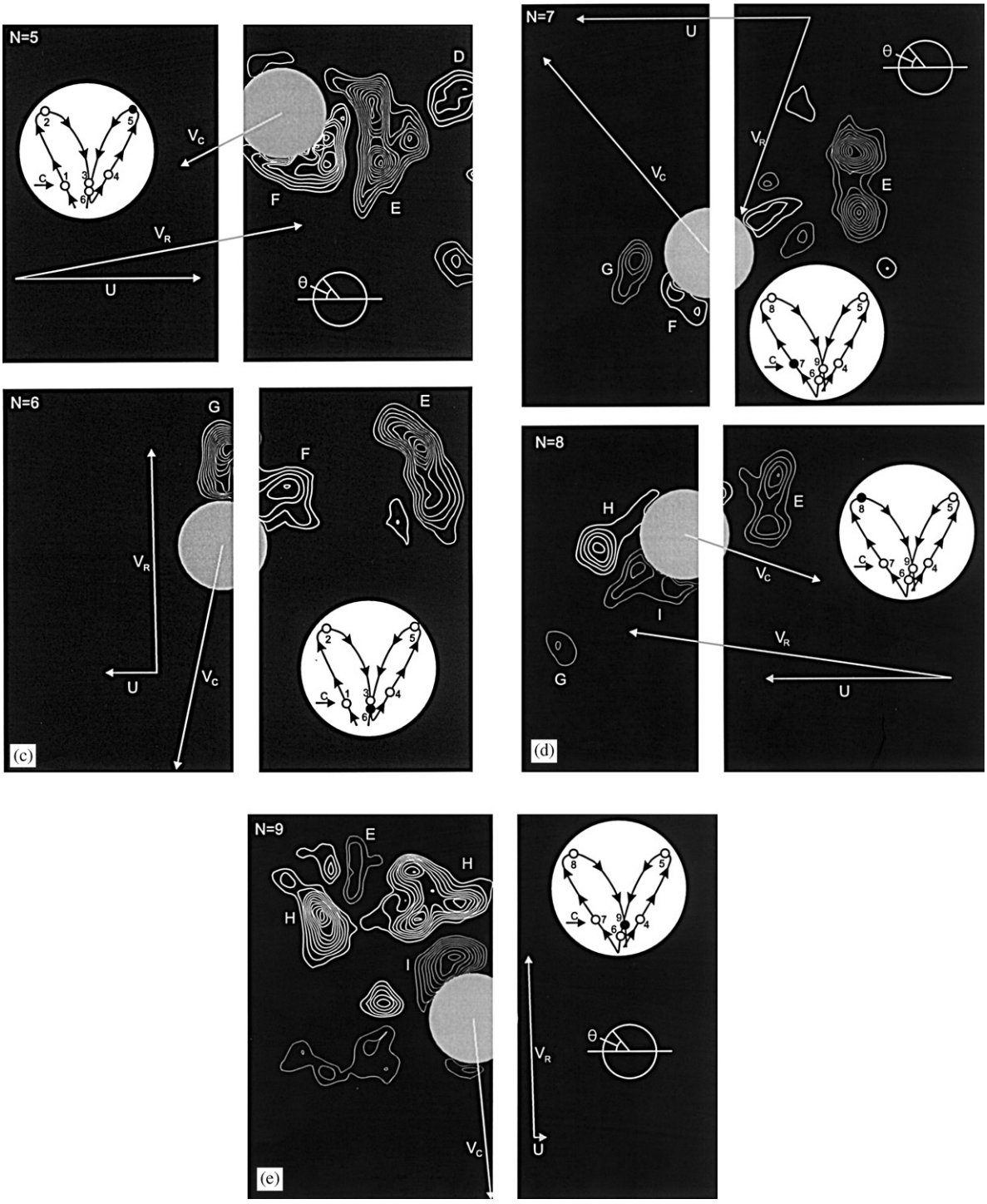

Fig. 3 (*continued*).

image $N = 3$. As a consequence, the vorticity concentration E has rotated in the clockwise direction about the surface of the cylinder, while remaining remarkably attached. In fact, comparison of images $N = 2$, 3, and 4 shows that the total angle of rotation of E is approximately 270°. The vorticity concentrations D have degenerated to a number of

smaller-scale entities; they lie in the path of the instantaneous cylinder motion. Finally, the strength of vorticity concentrations A and B has significantly diminished to the point where they are no longer detectable.

As the cylinder continues along the right branch of its trajectory, it attains the extreme position corresponding to image $N = 5$ in Fig. 3c. The direction of velocity V_C of the cylinder is now at $\theta = -27°$, i.e. it is rotated 164° from its position in the aforementioned image $N = 4$. Correspondingly, the wave velocity vector V_R relative to the cylinder is at $\theta = 170°$, representing a rotation of 54° relative to its orientation in image $N = 4$. This relative wave velocity vector V_R does, however, remain generally oriented to the right, which promotes formation of a new vorticity concentration F from the bottom surface of the cylinder. Meanwhile, concentration E has shed from the cylinder; this shedding process involves the agglomeration of three small-scale concentrations of vorticity within the boundary of the large-scale concentration E. The pattern of shedding of concentrations E and F is remarkably Kármán-like, i.e. similar to shedding in a free-stream of constant velocity.

Image $N = 6$ of Fig. 3c exhibits the consequence of continued motion of the cylinder, along the right branch of its trajectory, which produces an increased magnitude of the cylinder velocity V_C, in the direction of $\theta = -78°$. The relative velocity V_R, now is at $\theta = 89°$, which represents a counterclockwise rotation of 81° relative to its position in image $N = 5$. As a consequence, a new concentration G has formed and is about to be shed from the surface of the cylinder. Simultaneously, concentration F has rotated in the counterclockwise direction around the cylinder surface, while remaining generally attached to the surface. Concentration E has moved well away from the cylinder.

Subsequent figures corresponding to images $N = 7$–9, in Figs. 3d and e, represent excerpts from the second cycle of the cylinder oscillation. Image $N = 7$ is at an instant on the trajectory approximately corresponding to image $N = 1$. The large-scale concentration E, which is actually composed of two identifiable smaller concentrations, still persists from the previous cycle of oscillation. Moreover, vorticity concentrations F and G have been swept about the cylinder relative to their positions in image $N = 6$. Comparing with image $N = 1$, vorticity concentrations F and G are analogous, respectively, to B and A. Furthermore, concentration E is analogous to concentration C. Differences in the patterns can be attributed to the fact that images $N = 1$ and 7 are not at exactly the same position on the trajectory, and therefore the magnitudes and orientations of U, V_C and V_R differ. Moreover, three-dimensional effects give rise to subtle differences of vortex formation along the surface of the cylinder, as well as irregularities of the rate of decay of the shed vorticity concentrations.

Considering the next instant in this second cycle of the cylinder motion, represented by image $N = 8$, which approximately corresponds to an extreme position of the cylinder trajectory, the pattern of vorticity can be compared with that exhibited in image $N = 2$. The precise location of the cylinder on its trajectory and the values of U, V_C and V_R differ somewhat between images $N = 2$ and 8, but the overall patterns are similar. The general form of the vorticity concentrations E, G, H, and I in image $N = 8$ is similar to the form of the corresponding concentrations C, A, D, and E in image $N = 2$ and occur at remarkably similar positions relative to the cylinder.

The next instant of the second cycle of oscillation, represented by image $N = 9$ in Fig. 3e, can be compared with image $N = 3$ in Fig. 3b for the first cycle of oscillation, even though images $N = 3$ and 9 are at somewhat different locations in the trajectory. The two well-defined concentrations of vorticity H in image $N = 9$ are analogous to those designated as concentrations D in image $N = 3$. Moreover, concentration I has the same form and general position as that designated as E in image $N = 3$. Vorticity concentrations shed during previous cycles of the cylinder oscillation are not generally discernible, which suggests that they decay very rapidly.

A larger field of view of image $N = 9$ is provided in Fig. 4. Only a few small-scale vorticity concentrations are detectable outside of the original field of view, which reaffirms their rapid decay.

4.2. Overview of generation and development of patterns of vorticity

Viewing together the collection of vorticity images presented in the foregoing, along with the history of the cylinder motion about its trajectory, and the corresponding variations of the cylinder velocity V_C, wave velocity U, and wave velocity relative to the cylinder V_R, it is possible to arrive at general observations, which are summarized in the following.

4.2.1. Onset and development of large-scale vorticity concentrations

The generation and subsequent shedding of large-scale concentrations of vorticity involves several successive stages, which include: large values of relative velocity V_R; rapid changes in direction of the cylinder velocity V_C; and a nearly orthogonal relation between the relative velocity V_R and the absolute wave velocity U, when U approaches zero.

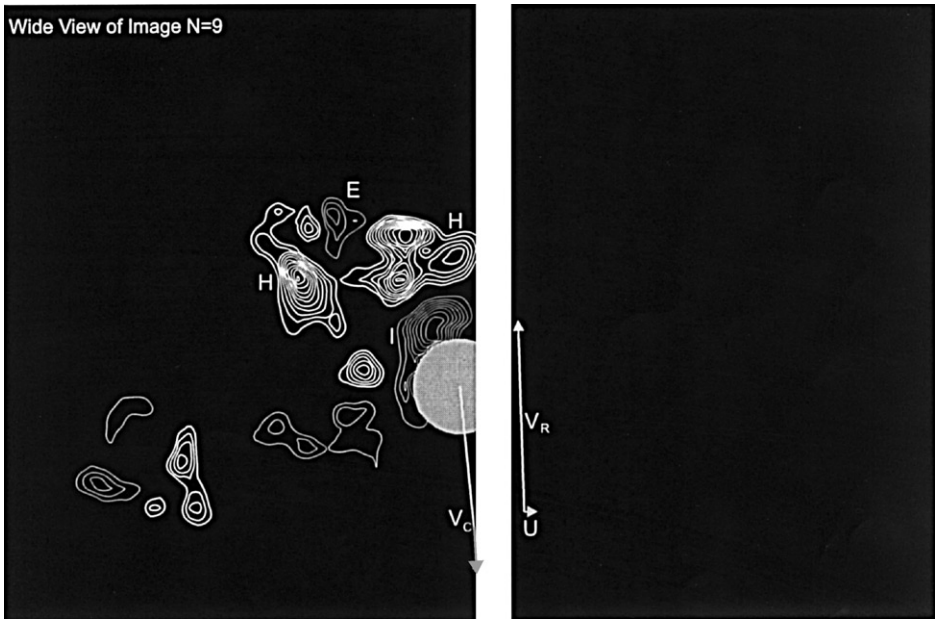

Fig. 4. Wide field of view of image $N = 9$ shown in Fig. 3e, which emphasizes rapid decay of vorticity concentrations.

More specifically, large-scale clusters of vorticity are evident in the form of concentrations D in images $N = 2$, 3 in the first cycle, and concentrations H in images $N = 8$, 9 in the second cycle of the cylinder motion. The onset of rapid growth of the concentrations D and H occurs when the relative velocity V_R attains its maximum value, due to the cylinder velocity V_C directly opposing the local particle velocity U of the wave, as exhibited in images $N = 2$ and 8. This attainment of maximum V_R is accompanied by a rapid change in direction of the cylinder velocity vector V_C, by nearly 180°; this is evident by comparing the direction of V_C in image $N = 3$ with that of $N = 1$, and in image $N = 9$ with that of $N = 7$. Finally, vorticity concentrations D, as well as H, attain full strength and are shed from the cylinder as the relative velocity vector V_R rotates to a direction orthogonal to the direction of the wave motion, as shown in images $N = 3$ and 9. Remarkably, at this phase of the cylinder trajectory, the wave velocity U goes to zero and the cylinder vector velocity V_C rotates normal to the direction of the wave, such that it opposes V_R.

The end consequence of the foregoing is, immediately upon completion of shedding, generation of large-scale concentrations of vorticity D (see image $N = 3$) having a dimensionless circulation of $\Gamma^* = \Gamma/\pi D U_{\max} = 0.922$. Correspondingly, vorticity concentration H (see image $N = 9$) has a dimensionless circulation of $\Gamma^* = \Gamma/\pi D U_{\max} = 1.222$. In this definition of Γ^*, the velocity $U_{\max}$ denotes the maximum value of the horizontal component of the wave velocity U over the period of the oscillation cycle. It should be noted that these values of Γ^* are commensurate with dimensionless values of circulation of Kármán vortices formed from a stationary cylinder, as determined by Green and Gerrard (1993), and vorticity concentrations shed from a stationary horizontal cylinder in a wave, as determined by Oshkai and Rockwell (1999). In other words, despite the large changes in direction and acceleration of the cylinder over these portions of the trajectory, the strength of the largest-scale vortices does not exceed that of Kármán vortices arising from a naturally occurring global instability of the near-wake of a stationary cylinder.

4.2.2. Nonunique states of vortex generation and development on symmetrical branches of the cylinder trajectory

Despite the nearly symmetrical left and right branches of the cylinder trajectory, indicated in the bottom half of Fig. 2, as well as in the insets of each of the PIV patterns of images of Figs. 3a–e, distinctly different mechanisms of vortex generation and development are observed at the mirror image locations on the left and right branches of the trajectory. That is, even though the relative orientations of the wave velocity U, cylinder velocity V_C, and relative velocity V_R of the wave with respect to the cylinder are maintained at mirror image locations on the left and right branches, the patterns of vorticity have basically different forms.

More specifically, images $N = 2$ and 5 represent the instantaneous positions of the cylinder at approximately mirror image locations of its trajectory; at these locations, the relative orientations of V_R, V_C, and U are essentially

the same, but the patterns of vorticity are fundamentally different. A similar comparison holds for images $N = 5$ and 8.

These observations suggest the importance of the history of the vortex formation process relative to the cylinder motion, thereby leading to nonunique states of vortex formation for a given combination of U, V_C and V_R. Of course, all previously formed concentrations of vorticity and their mutual induction contribute to the so-called history effect.

4.2.3. Collision of vorticity concentrations with surface of cylinder

A critical aspect of the aforementioned history effect appears to be the collision of previously formed vortices with the surface of the cylinder. Certain vortices that are formed during an earlier part of the cylinder trajectory move away from the cylinder by as much as two cylinder diameters, then collide with the cylinder at a later phase of the cylinder trajectory.

Details of this process are shown for the large-scale concentration of vorticity C in images $N = 1-3$ and concentration E in images $N = 5-9$. The collision occurs as the relative velocity V_R rotates nearly in-line with the wave velocity U. Furthermore, during the collision process, the value of V_R attains its maximum and exceeds the magnitude of U.

The collision process involves severe distension of the large-scale vortex about the surface of the cylinder and, except for a small remnant evident at a later phase in the cylinder trajectory ($N = 3$ and 9), the cluster of vorticity rapidly loses its identity.

4.2.4. Migration of large-scale vorticity concentrations about surface of cylinder

Not all large-scale concentrations of vorticity formed from the surface of the cylinder move away from the cylinder as it negotiates its trajectory. In fact, certain vorticity clusters remain attached to the cylinder surface and migrate, as much as 180°, about its periphery. This migration process is evident for vorticity concentration E, shown in images $N = 3$, 4 and concentration F in images $N = 6$ and 7. Such migration is associated with rapid changes in direction of the velocity vector V_C of the cylinder as, for example, occurs in going from $N = 3$ to 4. The vorticity concentrations remain remarkably attached to the surface of the cylinder.

Such attached concentrations of vorticity are expected, however, to exert a substantial contribution to the force vector. In accord with the concept of Lighthill (1986), the force associated with a given vorticity concentration is due to the time rate change of momentum of the vorticity concentration with respect to the center of the cylinder. During the migration about the periphery, the concentration can induce a substantial force, which rapidly changes direction as it rotates.

Particularly remarkable is the location of vorticity cluster E on the periphery of the cylinder, with respect to the relative velocity V_R. If it is assumed that the change in magnitude and orientation of V_R dictate the generation of vorticity, then the position of the vorticity cluster E in images $N = 2$, 3 and 4 retains the same relative orientation with respect to V_R, which undergoes several changes in angular displacement. That is, the angle θ of the center of the cluster E always lags the angle of inclination of V_R by about 70–90°. This condition is compatible with the continued generation from the surface of the cylinder. Furthermore, consider the dimensionless circulation Γ^* of cluster E. It shows substantial circulation $\Gamma^* = -0.699$ in $N = 3$ and $\Gamma^* = -0.509$ in $N = 4$, and the process of shedding yields $\Gamma^* = -0.936$ in $N = 5$.

4.2.5. Onset of short-term Kármán-like vortex shedding

Shedding of alternating concentrations of vorticity can occur at certain phases of the trajectory of the cylinder motion. Such shedding is evident in image $N = 5$, corresponding to the crest of the right branch of the trajectory. At this instant, the relative velocity of the wave V_R nearly opposes the cylinder velocity V_C.

The onset of this short duration version of Kármán-like shedding from the cylinder is remarkable, in that the effective KC number at this instant is relatively low, KC = 5.9. For the limiting case of simulated long-wave motion via unidirectional oscillatory flow, such as that generated in U-tube, it is well known that the first signs of a Kármán-like shedding occur at a higher value of KC = 8. This observation emphasizes the importance of the wave velocity relative to the cylinder moving along a bidirectional trajectory. For the present observations, this relatively large wave velocity V_R occurs when the wave velocity U directly opposes the cylinder velocity V_C.

Short-duration Kármán-like shedding also occurs for the scenario, where the cylinder velocity V_C has a large magnitude in the direction orthogonal to the direction of wave motion, i.e. at $N = 3$ and 9. At these instants, the absolute wave velocity U is minimum, leading to a large value of relative wave velocity V_R, i.e., in images $N = 3$ and 9, which is orthogonal to the direction of the absolute velocity U.

4.2.6. Rapid decay of vorticity concentrations

If the vortices formed from the cylinder were purely two-dimensional, one would expect their peak vorticity and circulation to decay relatively slowly, in accord with viscous diffusion. In contrast, it is evident from the excerpts shown in the present images that the vortices decay extremely rapidly and, in fact, only those that are formed during a given trajectory, or during a portion of the previous trajectory, are generally detectable in the images. Consider, for example, vorticity concentration D in image $N = 3$. It has a value of dimensionless circulation $\Gamma^* = 0.922$. Its circulation diminishes to $\Gamma^* = 0.267$ in image $N = 4$ and to $\Gamma^* = 0.148$ in $N = 5$. The elapsed time interval between the images $N = 3$ and 5 is 0.684 s, which corresponds to only 34% of both the cylinder oscillation cycle and the wave period. This decay is represented in a zoomed-out version of image $N = 9$, exhibited in Fig. 3e. It is evident that only a few, small-scale vorticity concentrations are detectable in the region well away from the cylinder. In fact, inspection of wide fields of view for all the remaining images shown in Fig. 3 reveals that only images $N = 3$, 6 and 9 show small-scale concentrations well away from the cylinder; all other images $N = 1$, 2, 5, 7, and 8 show no detectable concentrations of vorticity outside the field of view shown in Figs. 3a–d.

This rapid decay is also evident for other vorticity concentrations. Values of Γ^* were calculated for vorticity concentrations A–I in successive frames. If one considers the decay of Γ^* from its peak value to its value two frames later (two values of N later), the average decay is to 23.7% of the peak value. This decay occurs over approximately one-third of the oscillation cycle. These observations contrast with the wide variety of numerically computed vortex patterns from simulated or actual wave motion past a cylinder. In such simulations, an array of a large number of vorticity concentrations, extending over a domain well away from the center of the cylinder, are present due to the relatively slow process of vortex decay. It remains for further investigation to determine the origin of the rapid decay observed in the present case. It may be due to a combination of inherent, small-scale streamwise vorticity that would exist in a unidirectional wave flow, along with an effect due to the orbital trajectories of the actual, incident wave motion addressed in the present investigation.

5. Concluding remarks

An elastically mounted vertical cylinder in a free-surface wave gives rise to a generic form of vibrational trajectory. The cylinder has a very low value of mass-damping parameter and is configured such that its axis remains vertical over the entire trajectory of vibration. The trajectory has critical features in common with similar trajectories, as well as more complex forms of trajectories, observed in cantilevered, bidirectional elastic cylinder systems of relatively high mass-damping ratio. This generic trajectory allows assessment of the vortex development and interaction during the cylinder motion, with potential application of the fundamental observations to a broader range of related trajectories. The general form of the trajectory is the outline of the wing pattern of a moth or butterfly; this "butterfly" pattern is therefore symmetric with respect to a line of symmetry orthogonal to the direction of the wave motion.

The basic elements of vortex generation and development addressed in the preceding section are expected to be inherent features of cylinder trajectories more complicated than the generic trajectory considered herein. That is, the conditions for onset and development of large-scale vorticity concentrations, migration of large-scale concentrations about the periphery of the cylinder in conjunction with the direction of the relative velocity, occurrence of short duration Kármán-like shedding, and collision of previously formed vortices with the surface of the cylinder appear to be fundamental mechanisms. It has been demonstrated that use of a concept of relative wave velocity can explain these types of vortex generation and development. Particularly intriguing is the limiting case of large relative wave velocity in a direction orthogonal to the absolute local (particle) wave velocity; it occurs when the absolute wave velocity tends to zero. The interesting combinations of relative and absolute wave velocity also occur in relation to velocity of the cylinder. All result in generation of distinctive patterns of vorticity concentration.

It is important, however, to note that even when the instantaneous relative velocity, the absolute wave velocity, and the cylinder velocity have the same relative orientations and magnitudes, distinctly different patterns of vorticity are present. The history of the cylinder motion about its trajectory and thereby the corresponding history of the patterns of vorticity appears to be a key feature of this nonuniqueness.

Finally, the decay of the projection of the vorticity concentrations in the horizontal plane of observation is remarkably rapid for all phases of the oscillation cycle. It substantially exceeds that expected on the basis of diffusion effects, and is likely linked to the inherent three-dimensionality of the wave motion along the span of the cylinder.

Acknowledgements

The authors are pleased to acknowledge the financial support of the Office of Naval Research under Grant N00014-1-0815, monitored by Dr Thomas Swean. In addition, they are grateful to Dr Jung-Chang Lin for collaboration on several technical aspects of this project.

References

Adrian, R.J., 1991. Particle-imaging techniques for experimental fluid mechanics. Annual Review of Fluid Mechanic 23, 261–304.

Anagnostopoulos, P., Iliadis, G., Ganoulis, J., 1995. Flow and response parameters of a circular cylinder vibrating in-line with the oscillating stream. In: Bearman, P. (Ed.), Flow-Induced Vibration. Balkema, Rotterdam, pp. 167–179.

Angrilli, F., Cossalter, V., 1982. Transverse oscillations of a vertical pile in waves. Journal of Fluids Engineering 104, 46–53.

Bearman, P.W., Hall, P.F., 1987. Dynamic response of circular cylinders in oscillatory flow and waves. In: King, R. (Ed.), Proceedings of BHRA Conference on Flow-Induced Vibrations. BHRA, Bowness-on-Windermere, UK, Cranfield, pp. 183–190.

Bearman, P.W., Graham, J.M.R., Naylor, P., Obasaju, E.D., 1981 The role of vortices in oscillatory flow about bluff bodies. Proceedings of International Symposium on Hydrodynamics and Ocean Engineering, The Norwegian Institute of Technology, pp. 621–644.

Borthwick, A.G.L., Herbert, D.M., 1988. Loading and response of a small diameter flexibly mounted cylinder in waves. Journal of Fluids and Structures 2, 479–501.

Downes, K., 1999. Oscillations of a vertical elastically mounted cylinder in a wave. Master of Science Thesis, Lehigh University, Bethlehem, PA.

Downes, K., Rockwell, D., 1998. Wave interaction with a vertical, two-degree of freedom, elastically mounted cylinder. Bulletin of the American Physical Society 43 (9), 2071 Abstract No. JE7.

Green, R.B., Gerrard, J.H., 1993. Vorticity measurements in the near wake of a circular cylinder at low Reynolds number. Journal of Fluid Mechanics 246, 675–691.

Hayashi, K., Chaplin, J.R., 1998. Vortex-excited vibration of a vertical circular cylinder in waves. International Journal of Offshore and Polar Engineering 8, 66–73.

Honji, H., 1981. Streaked flow around an oscillating circular cylinder. Journal of Fluid Mechanics 107, 509–520.

Ikeda, S., Yamamoto, Y., 1981 Lift force on cylinders in oscillatory flows. Report of Department of Found. Engineering and Const. Engineering, Saitama University, No. 10.

Ippen, A.T., 1966. Estuary and Coastline Hydrodynamics. McGraw-Hill, New York.

Isaacson, M.DE ST.Q., Maull, D.J., 1981. Dynamic response of vertical piles in waves. International Symposium on Hydrodynamics in Ocean Engineering, The Norwegian Institute of Technology, Trondheim, Norway. pp. 887–904.

Iwagaki, Y., Asano, T., Nagai, F., 1983. Hydrodynamic forces on a circular cylinder placed in wave-current co-existing fields. Memo Faculty of Engineering (Kyoto University, Japan) 45, 11–23.

Kaye, D., 1989. Oscillation of a vertical cylinder in waves. Ph.D. Dissertation, University of Cambridge.

Kaye, D., Maull, D.J., 1993. The response of a vertical cylinder in waves. Journal of Fluids and Structures 7, 867–896.

Kozakiewicz, A., Sumer, B.M., Fredsøe, J., Hansen, E.A., 1997. Vortex regimes around a freely vibrating cylinder in oscillatory flow. International Journal of Offshore and Polar Engineering 7, 94–103.

Li, Y.S., Zhan, S., Lau, S.L., 1997. In-line response of a horizontal cylinder in regular and random waves. Journal of Fluids and Structures 11, 73–87.

Lighthill, J., 1986. Fundamentals concerning wave loading on offshore structures. Journal of Fluid Mechanics 173, 667–681.

Lipsett, A.W., Williamson, I.D., 1991. Modelling the response of flexibly mounted cylinders in oscillatory flow. Proceedings of the First International Offshore and Polar Engineering Conference, Edinburgh, UK, pp. 370–377.

Lipsett, A.W., Williamson, I.D., 1994. Response of a cylinder in oscillatory flow. Journal of Fluids and Structures 8, 681–709.

Obasaju, E.D., Bearman, P.W., Graham, J.M.R., 1988. A study of forces, circulation and vortex patterns around a circular cylinder in oscillating flow. Journal of Fluid Mechanics 196, 467–494.

Oshkai, P., Rockwell, D., 1999. Free surface wave interaction with a horizontal cylinder. Journal of Fluids and Structures 13, 935–954.

Rockwell, D., Lin, J.-C., Cetiner, O., Downes, K., Yang, Y., 2001. Quantitative imaging of the wake of a cylinder in a steady current and a wave. Journal of Fluids and Structures 15, 427–444.

Sarpkaya, T., 1986. Force on a circular cylinder in viscous oscillatory flow at low Keulegan–Carpenter numbers. Journal of Fluid Mechanics 165, 61–71.

Sarpkaya, T., Isaacson, M.DE ST.Q., 1981. Mechanics of Wave Forces on Offshore Structures. Van Nostrand Reinhold, New York.

Sarpkaya, T., Rajavi, F., 1979. Dynamic response of piles to vortex shedding in oscillatory flows. Proceedings of the 11th Offshore Technology Conference, Houston, Texas. OTC Paper 3647, pp. 2523–2528.

Sawaragi, T., Nakamura, T., Miki, H., 1977. Dynamic behavior of a circular pile due to eddy shedding in waves. Coastal Engineering in Japan 20, 109–120.

Sumer, B.M., Fredsøe, J., 1988. Transverse vibrations of an elastically mounted cylinder exposed to an oscillating flow. Journal of Offshore Mechanics and Arctic Engineering 110, 387–394.

Sumer, B.M., Fredsøe, J., 1997. Hydrodynamics Around Cylindrical Structures. World Scientific, London.

Tatsuno, M., Bearman, P.W., 1990. A visual study of the flow around an oscillation circular cylinder at low Keulegan–Carpenter numbers and low stokes numbers. Journal of Fluid Mechanics 211, 157–182.

Williamson, C.H.K., 1985a. Sinusoidal flow relative to circular cylinders. Journal of Fluid Mechanics 155, 141–174.

Williamson, C.H.K., 1985b. In-line response of a cylinder in oscillatory flow. Applied Ocean Research 7, 97–106.

Yang, Y., Rockwell, D., 2002. Wave interaction with a vertical cylinder: spanwise flow patterns and loading. Journal of Fluid Mechanics 460, 93–129.

Zedan, M.F., Yeung, J.Y, Salane, H.J., Fischer, F.J., 1981. Dynamic response of a cantilever pile to vortex shedding in regular waves. ASME Journal of Energy Resources Technology 103, 32–40.